*American Mineralogist, Volume 62, pages 857–873, 1977*

# Exsolution lamellae in augite and pigeonite: fossil indicators of lattice parameters at high temperature and pressure

PETER ROBINSON

*Department of Geology, University of Massachusetts*
*Amherst, Massachusetts, 01002*

MALCOLM ROSS, GORDON L. NORD, JR.

*U.S. Geological Survey, Reston, Virginia 22092*

JOSEPH R. SMYTH[1]

*Lunar Science Institute, Houston, Texas 77058*

AND HOWARD W. JAFFE

*Department of Geology, University of Massachusetts*
*Amherst, Massachusetts, 01002*

**Abstract**

Two geothermometers have been devised for determining exsolution temperatures in monoclinic pyroxene based on (1) the orientation of exsolution boundaries and (2) the differential changes in unit-cell sizes for host and lamellar phases during cooling.

Lamellar orientations are selected to minimize strain energy between host and lamellae. The orientations in clinopyroxene at different exsolution temperatures have been modeled under the condition that the $b$ dimensions of both phases are identical, thus the orientations are a function of only the differences $\Delta a$, $\Delta c$, and $\Delta\beta$ between host and lamellae. By slight lattice rotations, lamellar boundaries can be found that achieve perfect dimensional fit. These are termed "exact phase boundaries." For constant $\Delta\beta$, variation of $\Delta a$ by 0.20A can result in 18° variation in the angle of "001" lamellae and variation of $\Delta c$ by 0.20A can result in 32° variation in the angle of "100" lamellae. The orientations of exsolution lamellae vary with temperature. In the 50°C interval near the $C2/c \rightarrow P2_1/c$ transition this variation is particularly marked, due to the abrupt contraction of pigeonite lattice parameters.

The model has been used to determine the exsolution temperature of four different sets of pigeonite lamellae in augite from the Bushveld Main Zone Gabbro: 5 $\mu$m thick "001" pigeonite lamellae (Pig I, "001"$\Lambda c$ = 103°), formed near 1000°C, well above the $P$–$C$ transition; 0.5 $\mu$m thick "100" pigeonite lamellae ("100"$\Lambda c$ = −6°), formed near 850°C, above the $P$–$C$ transition; 1 $\mu$m thick "001" pigeonite lamellae (Pig II, "001"$\Lambda c$ = 106°), formed near 800°C, just above the $P$–$C$ transition; and 0.8 $\mu$m thick "001" pigeonite lamellae (Pig III, "001"$\Lambda c$ = 112°), formed near 560°, below the transition, as in most metamorphic augites.

Below the temperature of exsolution, additional lattice rotation occurs because $\beta$ of pigeonite decreases more rapidly than $\beta$ of augite, thus severely straining the confined pigeonite lamellae. The strain is relieved by formation of stacking faults on (100) of pigeonite. Both the stacking fault density observed on electron micrographs and the amount of $\beta$ decrease determined by X-ray and electron diffraction are potential independent geothermometers. The stacking faults may inhibit growth of lamellae, and this factor should be considered by those researchers attempting to model lamellae growth by bulk diffusion rates alone.

[1] Present address: Los Alamos Scientific Laboratory, P.O. Box 1663, Los Alamos, New Mexico, 87545

## Introduction

The nature of the orientation of exsolution lamellae in clinopyroxenes and clinoamphiboles has been discussed in two earlier papers. The first paper (Robinson *et al.*, 1971) demonstrated how the principle of optimal phase boundaries can be used to explain the irrational orientations that such lamellae commonly show, and developed some principles concerning the orientation of lamellae as a function of temperature and pressure conditions during phase separation. The second paper (Jaffe *et al.*, 1975) described the orientation of lamellae in augites from metamorphic rocks and demonstrated the relationship between the orientation of the lamellae and composition. In this paper we consider the nature of exsolution lamellae and their lattice orientations in augites from igneous rocks with a history of slow cooling from high temperature. The orientation of these exsolution features are dependent on the high-temperature lattice parameters and hence can be used as geothermometers.

## Structure of interphase boundaries

Interphase boundaries can be described as completely *coherent, semi-coherent,* or *incoherent,* and the boundary orientation is generally along the lowest energy configuration (Willaime and Brown, 1974). A completely coherent interface requires that the lattice planes of the host be continuous with, though not necessarily parallel to, the lattice planes of the precipitate. In this case the elastic energy of the boundary is a function of the lattice misfit and the stiffness anisotropy of the two phases, and is a minimum for certain orientations. The lattice misfit is a function of the lattice constants (Willaime and Brown's first postulate), while the stiffness anisotropy is a function of the elastic stiffness coefficients (Willaime and Brown's second postulate), all values being taken from the strain-free phases of appropriate compositions. In the semicoherent case, the strain due to the lattice misfit and elastic stiffness is relaxed within a few unit cells of the boundary (Aaronson *et al.*, 1970) by an array of interface dislocations, coherency being maintained only between the dislocations. In the incoherent case there is no correspondence of lattice planes across the interface boundary and the interfacial energy is effectively independent of orientation (Christian, 1965, p. 332).

In the present and previous studies (Robinson *et al.*, 1971; Jaffe *et al.*, 1975) the boundaries have been considered to have been coherent at the initiation of exsolution, even though they may have become semi-coherent or incoherent during subsequent cooling. The effect on boundary orientation caused by elastic stiffness anisotropy (as in Willaime and Brown's model) has been neglected in these studies. The justification for this is that the observed lamellar orientation appears to be adequately described using the Robinson *et al.* model, which suggests that for pigeonite exsolving from augite, elastic stiffness anisotropy plays a minor role. Willaime and Brown also found this to be true for most of the precipitate interface orientations in feldspars.

## Optimal and exact phase boundaries

Robinson *et al.* (1971) and Jaffe *et al.* (1975) showed that augite or pigeonite exsolution lamellae in a pigeonite or augite host initially form with coherent boundaries, the orientation of which is controlled by minimum strain considerations between host and lamellae, as determined by their difference in lattice parameters under the $P$–$T$ conditions during which exsolution occurred. In all pyroxenes thus far examined by us, the $b$ dimensions of the host and lamellae are identical ($\Delta b = 0$) within the accuracy of measurement (approximately ± 0.01 to 0.02 A). The orientation of the boundaries is thus a function of the differences between the unit-cell parameters $a$, $c$, and $\beta$ ($\Delta a$, $\Delta c$, $\Delta\beta$). Such boundaries have been termed by us "optimal phase boundaries" after the terminology of Bollmann and Nissen (1968). However, in most pyroxene pairs where $\Delta b = 0$, the phase boundaries are really much better than "optimal" (the best that can be achieved under the circumstances), because their orientation permits an *exact* lattice match at the two-phase interface. For this reason, we here term such phase boundaries which have perfect dimensional fit "exact phase boundaries."[2] Such exact dimensional fit is achieved between two *monoclinic* lattices, where $\Delta b = 0$, by the selection of two special irrational phase boundaries, one nearer to (001), termed "001", and one nearer to (100), termed "100", *and* by slight relative rotation of the two crystal lattices (Robinson *et al.*, 1971, Fig. 6; Jaffe *et al.*, 1975, p. 22–23). This type of rotation is here called "phase-boundary lattice rotation" to distinguish it from other types of lattice rotation that may take place well after exsolution, as will be described below. Four examples of such exact phase boundaries and phase-boundary lattice rotations for two different

[2] A method of calculating the orientation of the exact phase boundaries between two monoclinic phases is given in the Appendix.

pairs of lattices are shown in Figure 1.[3] Note that the lattice parameters of each pair of lattices uniquely determine the orientation of the two exact phase boundaries, and the amount and direction of phase-boundary lattice rotation.

As shown in Figure 1, at constant $\Delta\beta$, variation of $\Delta a(a_{AUG} - a_{PIG})$ from +0.10A to −0.10A results in variation in angle of "001" phase-boundaries in augite from +9.93 to −7.91°; variation of $\Delta c(c_{AUG} - c_{PIG})$ from +0.10A to −0.10A results in variation in angle of "100" boundaries from +17.19 to −14.97°. The greater the $\Delta a$ or $\Delta c$ between host and lamellae, the greater the deviation of the phase boundaries from the rational planes (001) and (100) respectively. When $\Delta a$ and $\Delta c$ are held constant, $\Delta\beta$ has an important opposite effect: as $\Delta\beta$ becomes *smaller* the deviation of the lamellae from (001) and (100) becomes *larger*. Thus, if $\Delta a$, $\Delta c$, $\Delta\beta$ are *all* decreased *systematically* at constant $T$, the orientation of the exact phase boundary with respect to the two lattices will tend to remain fairly constant even to the point where $\Delta a$, $\Delta c$, and $\Delta\beta$ (and the change in wollastonite content, $\Delta$Wo) approach zero (Table 1). Hence, the lattice parameters under the conditions of phase-boundary formation determine or strongly influence the orientation, regardless of the mechanism by which phase separation takes place and even in cases where differences between lattice parameters are exceedingly slight.

### Pyroxene lattice parameters at high temperature

Lattice parameters of clinopyroxenes are complex functions of composition, temperature, pressure, and structural state, any or all of which can become involved in determining the orientation of exact phase boundaries. The Ca-rich pyroxenes of the pyroxene quadrilateral (Fig. 2) show a systematic gradual increase in $a$ and $c$ with increasing $T$, but little change in $\beta$ (Cameron *et al.*, 1973). The Ca-poor clinopyroxenes (pigeonites), on the other hand (Fig. 3), show more rapid increases in $a$ and $c$ with increasing $T$, and in the 50°C interval near the nonquenchable $P2_1/c \rightarrow C2/c$ transition, $a$, $c$, and $\beta$ all increase dramatically (Smyth, 1974). Thus, well above the transition temperature, $a$ and $c$ of pigeonite are larger than $a$ and $c$ of augite (as in Fig. 1B), whereas well below the transition temperature, $a$ and $c$ of pigeonite are smaller (as in Fig. 1A). These differences affect the orientation of phase boundaries (Fig. 1), so that lamellae formed above or below the transition temperature can often be recognized, as can lamellae formed near the transition temperature. The orientations of pigeonite lamellae in augite and vice versa are thus a unique function and, if preserved, provide a fossil record of the lattice parameters at the conditions where phase separation first occurred on a particular phase boundary.

### Patterns of high temperature exsolution and their origin

Once a phase boundary has formed, the lamella can grow in thickness perpendicular to the boundary as long as changes in lattice parameters resulting from cooling and composition change do not cause large strains to develop and all other factors are favorable. Perpendicular growth on lamella phase boundaries in pyroxenes and amphiboles takes place by the lateral migration of ledges (Champness and Lorimer, 1973; Copley *et al.*, 1974; Gittos *et al.*, 1974). The ledge mechanism, however, can be impeded, and thus growth stopped, if the dislocations at the interface become immobilized or if the necessary solute is depleted at the interface (Aaronson *et al.*, 1970). One or both of these factors must have caused perpendicular growth to cease in the examples discussed below. During cooling the lamellae may, however, still propagate longitudinally into new material, by changing the phase-boundary orientation to suit the changing lattice parameters. Thus, lamellae having curved ends are formed that provide a *continuous* record of changing lattice parameters for continuously changing conditions (Fig. 4).

Eventually, possibilities for perpendicular and longitudinal growth may be exhausted, and the situation is set for nucleation of a new set of lamellae with

[3] Note that the phase boundaries in Fig. 1A and C can be described in terms of positive intercepts on the $a$ and $c$ crystallographic axes of the reference phase (Jaffe *et al.*, 1975, Table 5), whereas the phase boundaries in Fig. 1B and D require negative *and* positive intercepts. Thus the angles of phase boundaries that can have all positive intercepts and lie in the acute angle $\beta$ ($180° - \beta$) are treated as positive (Fig. 1A and C), whereas the angles of phase boundaries that require negative and positive intercepts and lie in the obtuse angle $\beta$ are treated as negative. In the case of "001" lamellae it is also convenient to express the orientation angle in the same terms as the angle $\beta$ of the reference phase to which the orientation angle has been added (+ or −). The same sign convention is adopted to describe "phase-boundary lattice rotation" or other orientations, except that the angle is taken as the angle that one direction in pigeonite makes with the equivalent direction in augite, using augite as the reference phase. Thus in Fig. 1A $a_{PIG}\Delta a_{AUG} = +0.40°$, whereas in Fig. 1B $a_{PIG}\Delta a_{AUG} = -0.04°$. This convention, deriving directly from the nature of intercepts, obviates the use of terms such as clockwise and anticlockwise that depend on the direction from which the lattice is viewed.

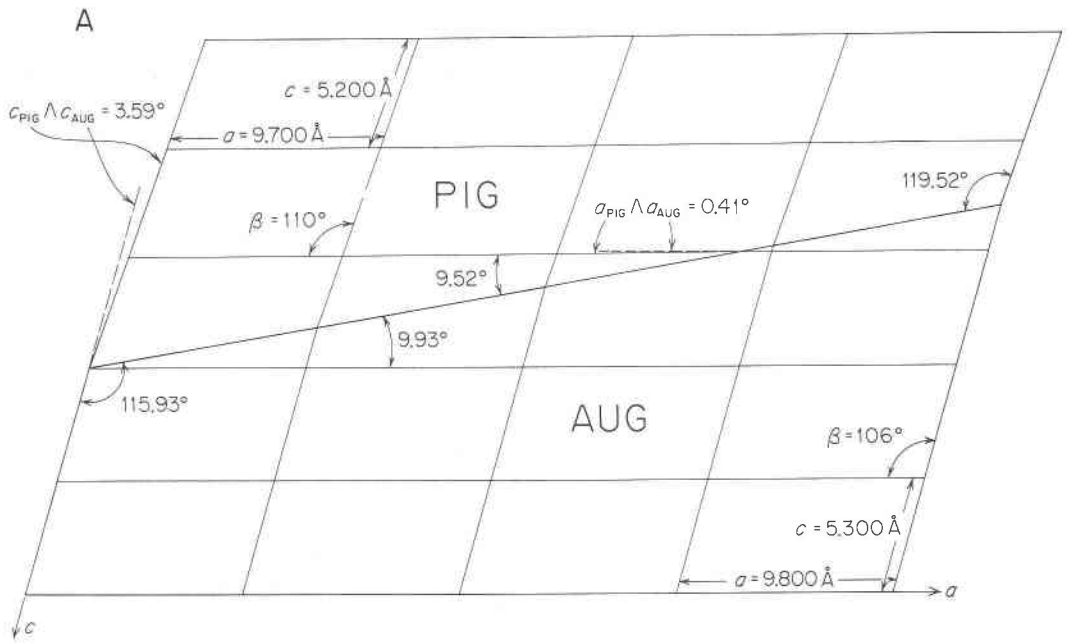


Fig. 1A. Scale drawing of model exact phase boundary. "001" boundary where $a_{AUG} > a_{PIG}$. $a_{PIG} \Lambda a_{AUG}$ is "phase-boundary lattice rotation" (see text).

different phase boundaries in the supersaturated regions located far from earlier lamellae. These new lamellae will have a slightly different orientation, reflecting the changed lattice parameters, which are due to lower temperature and/or pressure and changed composition (Fig. 4). In this way, a second and even a third generation (Fig. 5) of lamellae of different size and orientation can form within a single relatively homogeneous host. Natural examples of such multi-generation exsolution known to us are listed in Table

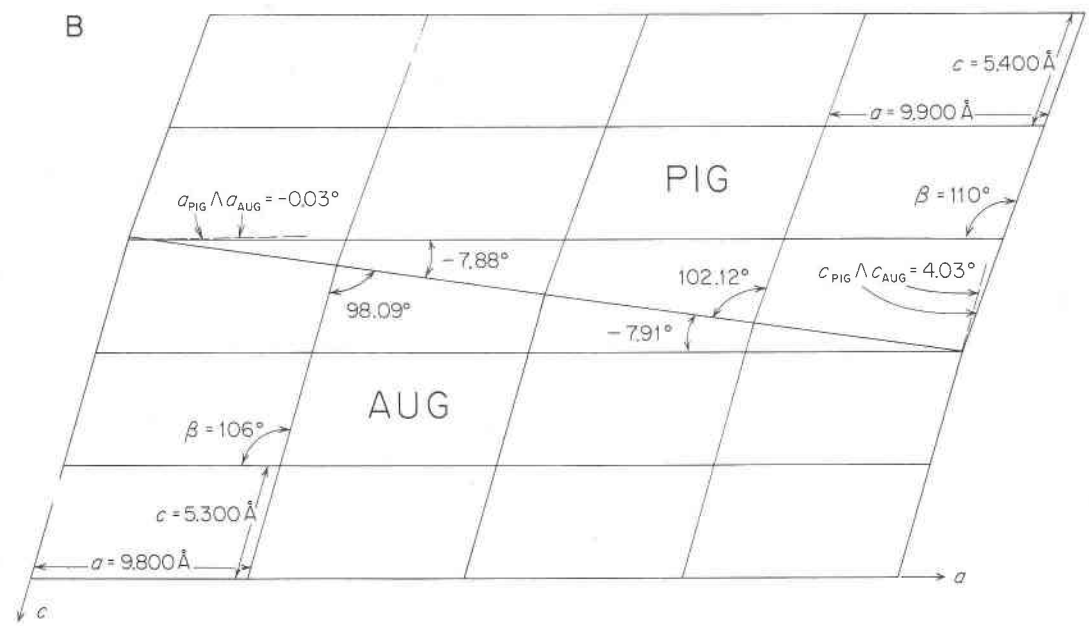


Fig. 1B. Scale drawing of model exact phase boundary. "001" boundary where $a_{AUG} < a_{PIG}$. $a_{PIG} \Lambda a_{AUG}$ is "phase-boundary lattice rotation" (see text).

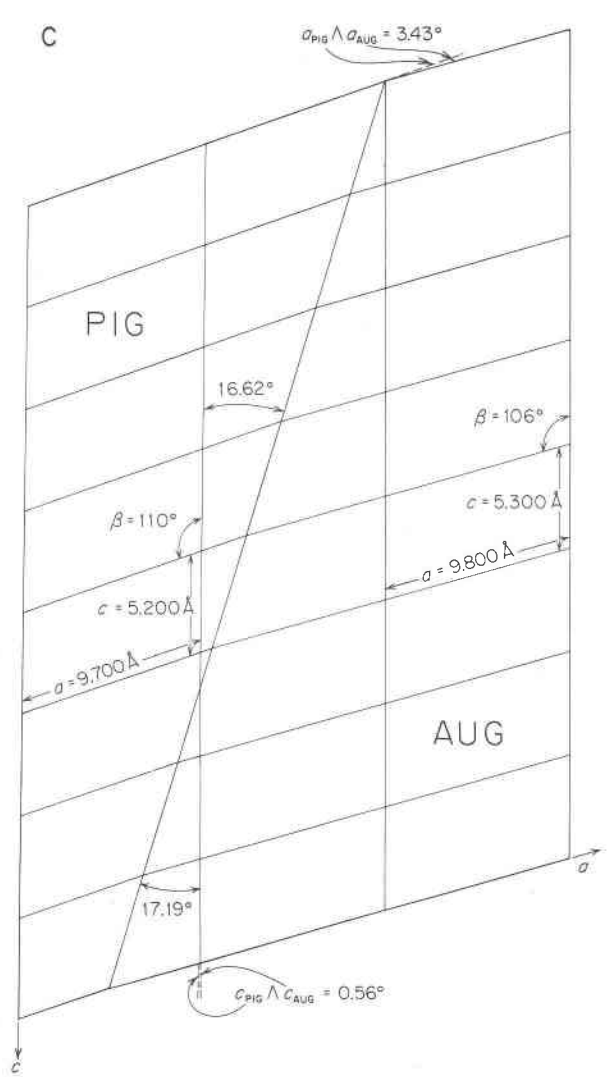


Fig. 1C. Scale drawing of model exact phase boundary. "100" boundary where $c_{AUG} > c_{PIG}$. $c_{PIG} \wedge c_{AUG}$ is "phase-boundary lattice rotation" (see text).

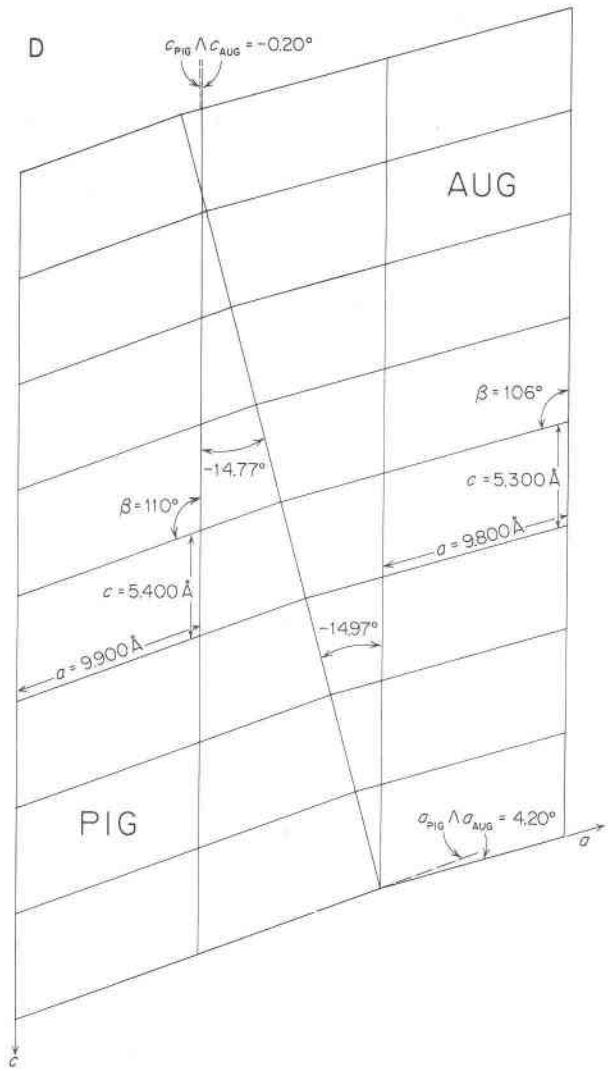


Fig. 1D. Scale drawing of model exact phase boundary. "100" boundary where $c_{AUG} < c_{PIG}$. $c_{PIG} \wedge c_{AUG}$ is "phase-boundary lattice rotation" (see text).

Table 1. Model lattice parameters and calculated phase boundaries to demonstrate lattice control on boundary orientation where $\Delta a$, $\Delta c$, $\Delta\beta$ (and $\Delta$Wo) approach zero

| $\Delta$Wo | $\underline{a}_{AUG}$ | $\underline{c}_{AUG}$ | $\beta_{AUG}$ | $\underline{a}_{PIG}$ | $\underline{c}_{PIG}$ | $\beta_{PIG}$ | $\Delta\underline{a}$ | $\Delta\underline{c}$ | $\Delta\beta$ | "001" Angle | "100" Angle |
|---|---|---|---|---|---|---|---|---|---|---|---|
| 50 | 9.847 | 5.280 | 105.76 | 9.877 | 5.335 | 110.26 | 0.03 | 0.055 | 4.5° | 103.6° | -7.5° |
| 40 | 9.848 | 5.280 | 105.80 | 9.872 | 5.324 | 109.40 | 0.024 | 0.044 | 3.6° | 103.7° | -7.5° |
| 30 | 9.848 | 5.281 | 105.99 | 9.866 | 5.303 | 108.69 | 0.018 | 0.033 | 2.7° | 103.8° | -5.0° |
| 10 | 9.850 | 5.284 | 106.50 | 9.856 | 5.2895 | 107.40 | 0.006 | 0.011 | 0.9° | 104.0° | -3.8° |
| 3 | 9.853 | 5.289 | 107.50 | 9.8548 | 5.2908 | 107.77 | 0.0018 | 0.0033 | 0.27° | 105.3° | -4.1° |
| 1 | 9.855 | 5.291 | 107.90 | 9.8556 | 5.2921 | 107.99 | 0.0006 | 0.0011 | 0.09° | 105.8° | -7.5° |
| 50 | 9.847 | 5.280 | 106.00 | 9.877 | 5.335 | 110.50 | 0.03 | 0.055 | 4.5° | 103.9° | -7.5° |
| 40 | 9.848 | 5.280 | " | 9.872 | 5.324 | 109.60 | 0.024 | 0.044 | 3.6° | 103.9° | -7.5° |
| 30 | 9.848 | 5.281 | " | 9.866 | 5.303 | 108.70 | 0.018 | 0.033 | 2.7° | 103.8° | -5.0° |
| 10 | 9.850 | 5.284 | " | 9.856 | 5.2895 | 106.90 | 0.006 | 0.011 | 0.9° | 103.8° | -3.8° |
| 3 | 9.853 | 5.289 | " | 9.8548 | 5.2908 | 106.27 | 0.0018 | 0.0033 | 0.27° | 103.9° | -4.1° |
| 1 | 9.855 | 5.291 | " | 9.8556 | 5.2921 | 106.09 | 0.0006 | 0.0011 | 0.09° | 103.9° | -7.5° |

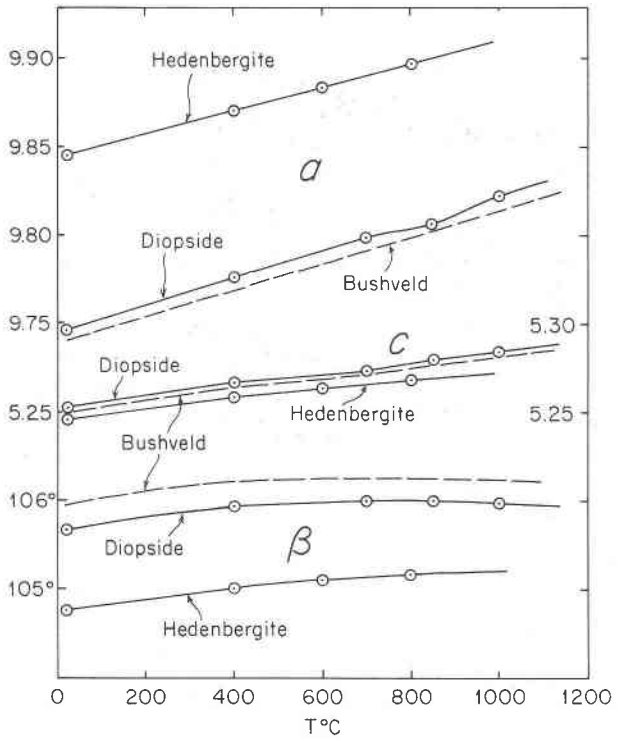


Fig. 2. Lattice parameters of Ca-rich pyroxenes measured at temperature ($T$). Dashed line is interpolated curve for Bushveld composition. Experimental points are from Cameron *et al.* (1973).

2. Specimen SA-1019 from the Bushveld Main Zone Gabbro, for which the most abundant information is available, is described in detail below.

### Bushveld augite

A polished thin section of specimen SA-1019 Main Zone Gabbro from the Bushveld Complex was kindly loaned to us by F. R. Boyd, Geophysical Laboratory. The augite host and pigeonite lamellae have been analyzed by Boyd and Brown (1969). The probe section proved to have the first-reported and most spectacular example of augite with three different sets of pigeonite "001" lamellae. A small chip of the rock was subsequently sent to us by G. M. Brown (University of Durham) from which single crystals were selected for X-ray study and thin sections were made for transmission electron microscopy (TEM). A preliminary report on optical and X-ray observations was given by Ross (1972). In addition, Champness and Copley (1976) have reported some TEM observations on the pyroxene microstructures found in specimen SA-1019.

The Bushveld augite is illustrated in Figure 5, and in photomicrographs in Figure 6; all are sections parallel to (010). The coarsest and earliest exsolution lamellae are "001" pigeonite, designated Pig-I, which are as thick as 12 $\mu$m with boundaries oriented at about 103° to the $c$ axis of the augite host (Fig. 5). These boundaries thus fall in the same class as the boundary illustrated in Figure 1B, and presumably formed at temperatures well above the $P2_1/c \rightarrow C2/c$ transition where $a_{AUG} < a_{PIG}$. A second coarse set of lamellae, 5 $\mu$m thick, appears to be parallel to (100). In some crystals these lamellae pass entirely through the "001" pigeonite lamellae, but bend 3–4° in crossing the pigeonite boundary, so that they also appear to be true (100) lamellae with respect to the pigeonite lattice. These lamellae are orthopyroxene.

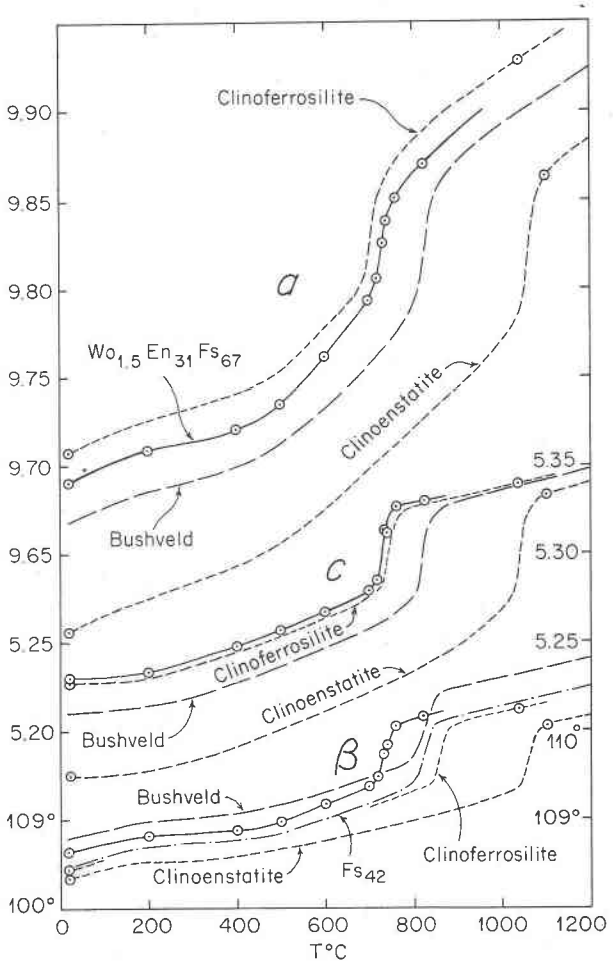


Fig. 3. Lattice parameters of Ca-poor clinopyroxenes (pigeonites) measured at temperature ($T$). Dash-dot curve is interpolated for pigeonite $Fs_{42}$ and the curve with long dashes is interpolated for Bushveld composition. Experimental points for $Wo_{1.5}En_{31}Fs_{67}$ are from Smyth (1974). Points for clinoenstatite and clinoferrosilite are from J. V. Smith (1969) and J. J. Papike (personal communication, 1973). Abrupt change in slope near 700°C indicates region of symmetry change, $P2_1/c$ below, $C2/c$ above.

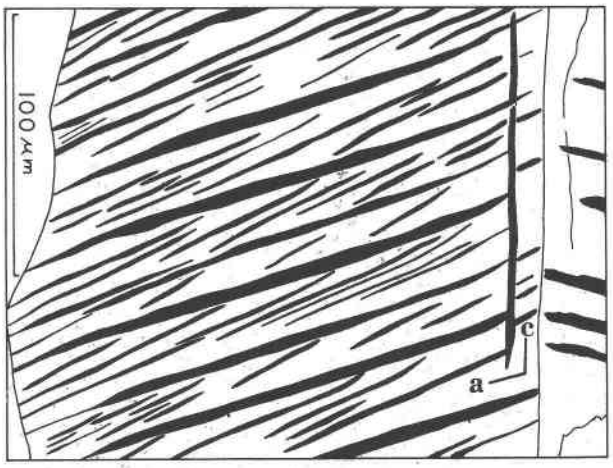


Fig. 4. Pattern of pigeonite exsolution lamellae in an (010) section of host augite from chill zone gabbro, Stillwater Complex, Montana. Two sets of lamellae, one at about 106° and the other at 115° to the *c*-crystallographic axis, each show curvature at the ends. The curvature is believed due to longitudinal growth during cooling and/or composition change that gradually changed the lattice parameters.

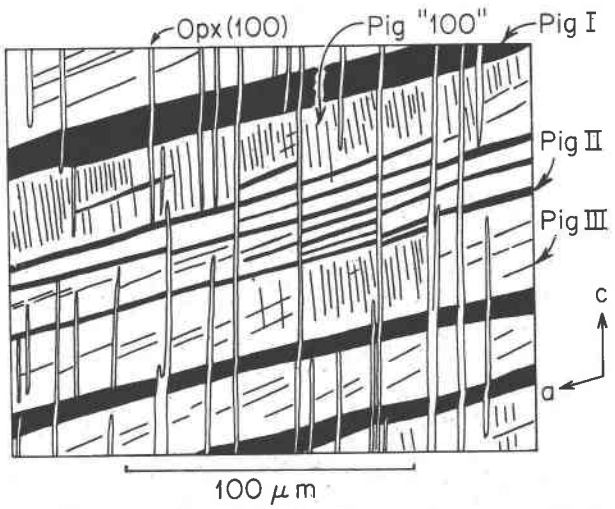


Fig. 5. Pattern of exsolution lamellae in (010) section of Bushveld augite (SA-1019) showing three generations of "001" pigeonite exsolution lamellae. "001" lamellae are coarse Pig I at 103° to the *c* axis of augite, medium-sized Pig II at 106° to the *c* axis, and fine Pig III at 112° to the *c* axis. Also present are pigeonite (Pig) "100" lamellae at −6° and orthopyroxene (Opx) (100) lamellae (unshaded) parallel to the *c* axis. Where orthopyroxene lamellae pass through Pig I lamellae they bend 3–4° so that they are parallel to (100) of the pigeonite of the lamella.

A second set of pigeonite "001" lamellae (Pig-II), 1–2 μm thick, having boundaries oriented at about 106° to the *c* axis of augite, usually occurs in groups of two to four lamellae at a position approximately halfway between coarse Pig-I lamellae. These boundaries are intermediate in character between the two classes illustrated in Figures 1A and 1B, and presumably formed under conditions in the general vicinity of the $P2_1/c \rightarrow C2/c$ transition where $a_{AUG} = a_{PIG}$. The third set of pigeonite "001" lamellae (Pig-III), about 0.5 μm thick, with boundaries oriented at about 112° to the *c* axis, occurs in the regions between Pig-I and Pig-II lamellae, and between pairs of Pig-I or Pig-II lamellae. In some cases (Fig. 6) Pig-III lamellae are merely longitudinal extensions of Pig-II lamellae and exhibit a continuum of angles from 106° to 112°. The boundaries of Pig-III lamellae fall in the same class as the boundary illustrated in Figure 1A and presumably formed under conditions below the $P2_1/c \rightarrow C2/c$ transition where $a_{AUG} > a_{PIG}$.

Within areas where other lamellae are scarce "100" pigeonite lamellae less than 0.5 μm thick are oriented at −6° to the *c* axis of augite. Although size criteria might suggest that these Pig "100" lamellae were contemporaneous with the Pig-III lamellae, the boundaries of the Pig "100" lamellae fall in the same class as the boundary illustrated in Fig. 1D, and would appear to have formed under conditions above the $P2_1/c \rightarrow C2/c$ transition where $c_{AUG} < c_{PIG}$. Fig-

Table 2. Examples of natural pyroxenes containing two or three generations of exsolution lamellae distinguished by orientation

| Source and Reference | Host Pyroxene | Lamellae "001" I | II | III | "100" |
|---|---|---|---|---|---|
| Duluth Gabbro, Minn., Robinson et al. (1971) Fig. 7. | Augite | 108° | 111–115° | | |
| Bushveld Main Zone Gabbro, SA-1019, Boyd and Brown (1969) and this paper. | Augite $Wo_{44}En_{38}Fs_{18}$ | 103° | 106° | 112° | −6° |
| Gabbro, Inner Border Z., Kiglapait Intrusion, Labrador, J.H. Berg, pers. comm. 1972 | Augite $Wo_{38}En_{38}Fs_{24}$ | 103° | 107° | 112° | 0° |
| Stillwater Complex, Mont., Chill Z. Gabbro, this paper; Hess (1960) | Augite $Wo_{41}En_{41}Fs_{18}$ | ∿106° | ∿115° | | |
| Ferromangerite Gneiss, Adirondacks, N.Y., Jaffe et al. (1975) | Augite $Wo_{44}En_{10}Fs_{46}$ | 111.5° | 112° | | 0° |
| | Augite $Wo_{42}En_{3}Fs_{55}$ | 111° | 112.5° | | |
| Moore County Meteorite; Morimoto and Tokonami (1969), Takeda (1972), Ross, unpub. data. | Pigeonite $Wo_{6}En_{48}Fs_{46}$ | 106° | 108° | | |
| Gabbro, Upper Border Z., Kiglapait Intrusion, Lab., W.A. Rewinski, pers. comm. 1975 | Augite $Wo_{44}En_{34}Fs_{22}$ | 104° | 112° | | |
| | Augite $WO_{43}En_{30}Fs_{27}$ | 108° | 112° | | −5° |
| | Augite $Wo_{42}En_{24}Fs_{34}$ | 112° | | | |

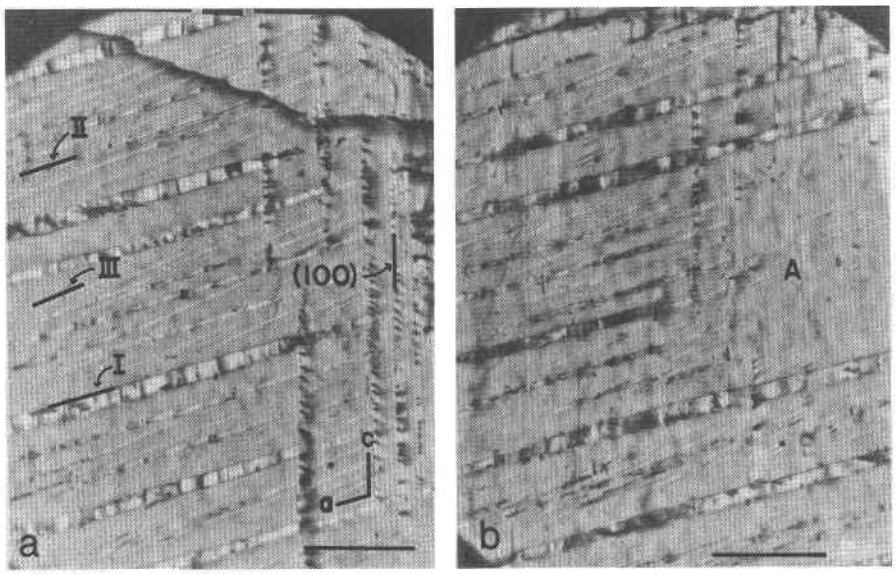


Fig. 6. Photomicrographs of exsolution lamellae in Bushveld augite. (a) Region dominated by three generations of pigeonite "001" lamellae, with coarse (100) orthopyroxene lamellae to right; $a$ and $c$ axes of augite are indicated. (b) Showing area (A) dominated by pigeonite "100" lamellae that is not penetrated by Pig II lamellae. Scale bar is 50 $\mu$m.

ure 6b shows a large area of Pig "100" lamellae that is completely free of Pig-II lamellae. Presumably Pig "100" lamellae formed before Pig-II lamellae and inhibited their later formation in this region. If correct, why are such earlier "100" lamellae so much finer than the later "001" lamellae? One possibility is that the growth rates are interface controlled, "001" interfaces growing more rapidly than "100" interfaces.

Unit-cell parameters for several augite crystals and included lamellae are given in Table 3. Crystal 1A showed reflections from all of the five sets of lamellae mentioned above, but the reflections from Pig "100" were too faint to permit measurement of the unit-cell parameters except $\beta$. Crystal 3A showed no reflections from Pig-II. Reflections from the three sets of pigeonite "001" lamellae were distinguished on the basis of relative intensities and on the basis of the orientation angles $a_{\mathrm{PIG}} \Lambda a_{\mathrm{AUG}}$ and $c_{\mathrm{PIG}} \Lambda c_{\mathrm{AUG}}$, a matter taken up in more detail below.

When phase-boundary angles are calculated from the observed room temperature unit-cell parameters of the Bushveld specimen (Table 4), the calculated angles from Pig-III data are close to those of the observed phase boundaries, suggesting that only relatively minor changes in unit-cell parameters occurred after exsolution. Such agreement between the calculated and observed angles of phase boundaries was found to be common in the case of metamorphic augites (Jaffe *et al.*, 1975). In contrast, however, the calculated angles using Pig-I and Pig-II data are far from the observed angles of 103° and 106°, respectively, indicating that the observed phase boundaries of the Pig-I and Pig-II lamellae formed when unit-cell parameters were quite different from what they are now. The observed phase boundaries appear to be a fossil record of those earlier unit-cell parameters and temperature conditions. For this reason, it seemed worthwhile to explore the relations between unit-cell parameters and temperature for the Bushveld composition join.

### Temperature–composition model for unit-cell parameters on the Bushveld SA-1019 join

The compositions of Bushveld augite and coarse pigeonite (Pig-I) lamellae obtained from probe analyses by Boyd and Brown (1969) are plotted on the pyroxene quadrilateral in Figure 7. These compositions define a low-temperature tie-line along the join $Di_{72}He_{28}$–$En_{58}Fs_{42}$. As augite (or pigeonite) unmixes during slow cooling there is generally a continuous change in the $Mg/Fe^{2+}$ ratio and calcium content of both the host and exsolved pyroxene. These subsolidus chemical reactions produce with decreasing temperature a lengthening of the tie-lines but very little tie-line rotation (Ross *et al.*, 1973; Ross and Huebner, 1975; M. Ross, unpublished data). The absence of appreciable tie-line rotation for coexisting

Table 3. Crystal mode and unit-cell parameters of host Bushveld augite and included lamellar pyroxenes*

| | a | c | β | Δa | Δc | Δβ |
|---|---|---|---|---|---|---|
| CRYSTAL 1A | | | | | | |
| Augite Host 79% | 9.742 | 5.254 | 105.96° | | | |
| Pig "001" I 7% | 9.669 | 5.208 | 108.78° | 0.073 | 0.046 | 2.82° |
| Pig "001" II 4% | 9.667 | 5.212 | 108.62° | 0.075 | 0.042 | 2.66° |
| Pig "011" III 7% | 9.694 | 5.216 | 108.96° | 0.048 | 0.038 | 3.00° |
| Pig "100" tr | | | 108.85° | | | |
| Opx (100) 3% | 18.249 | 5.253 | | | | |
| CRYSTAL 3A | | | | | | |
| Augite Host 80% | 9.741 | 5.246 | 105.92° | | | |
| Pig "001" I 12% | 9.671 | 5.218 | 108.70° | 0.070 | 0.028 | 2.78° |
| Pig "001" III 4% | 9.678 | 5.209 | 108.93° | 0.054 | 0.037 | 3.01° |
| Pig "100" 3% | 9.662 | 5.250 | 108.95° | 0.079 | | 3.03° |
| Opx (100) 1% | 18.278 | 5.251 | | | | |
| CRYSTAL 5A | | | | | | |
| Augite Host | | | 105.95° | | | |
| Pig "001" I | | | 108.85° | | | 2.90° |
| Pig "001" II | | | 108.93° | | | 2.98° |
| Pig "100" | | | 109.08° | | | 3.13° |
| CRYSTAL 6A | | | | | | |
| Augite Host | | | 106.07° | | | |
| Pig "001" I | | | 108.77° | | | 2.70° |
| Pig "001" III | | | 109.08° | | | 3.01° |

* Data from single crystal x-ray precession photographs, estimated error in the unit-cell edges is ± 0.3% and for the β angle ± 0.2°, b = 8.944 Å for all phases in crystal 1A and 3A, Δb = 0.

Table 4. Observed, calculated, and model phase boundaries for Bushveld augite

| Lamellae* | Observed | Calculated from RT Parameters Crystal 1A | Crystal 3A | Calculated from Model Parameters at T |
|---|---|---|---|---|
| Pig I | 103° | 115.6° | 114.9° | 1050°C 102.9° |
| | | | | 1000°C 102.9° |
| | | | | 900°C 103.5° |
| Pig II | 106° | 116.4° | | 800°C 106.2° |
| Pig III | 112° | 111.8° | 112.4° | 600°C 111.5° |
| Pig "100" | -6° | | -0.88° | 850°C -6.0° |
| Lamellae+ | | | | |
| Pig I | 107° | 118.1° | 117.5° | 1050°C 107.1° |
| | | | | 1000°C 106.4° |
| | | | | 900°C 106.3° |
| Pig II | 109° | 118.8° | | 800°C 109.5° |
| Pig III | 114° | 114.6° | 115.3° | 600°C 114.5° |
| Pig "100" | No Data | | -0.85° | 850°C -5.9° |

* Angles with respect to c-crystallographic axis of augite host

+ Angles with respect to c-crystallographic axis of pigeonite lamellae

pyroxene pairs with changing temperature simplifies the task of relating unit-cell parameters, composition, and temperature.

The data of Turnock *et al.* (1973), interpolated along the join $Di_{72}He_{28}$–$En_{58}Fs_{42}$, were used to define the room-temperature relationships between composition and unit-cell dimensions for the model Bushveld pyroxenes. Relations between unit-cell parameters and temperature for diopside and hedenbergite were taken from Cameron *et al.* (1973). For Ca-poor clinopyroxene, the relations between unit-cell parameters and temperature were taken from the data of Smyth (1974) on composition $Wo_{1.5}En_{31}Fs_{67}$. No other work on Ca-poor clinopyroxene is sufficiently detailed in the region of the $P2_1/c \rightarrow C2/c$ transition. Individual measurements at high temperature for clinoenstatite (Smith, 1969) and clinoferrosilite (J. J. Papike, personal communication, 1973) were also used. These experimental unit-cell data for high-Ca and low-Ca clinopyroxenes were plotted in Figures 2 and 3 respectively, and interpolated curves for $He_{28}$ and $Fs_{42}$ compositions were generated, using the data of Prewitt et al., (1971) to estimate $P2_1/c \rightarrow C2/c$ transition temperatures. The room temperature ends of these curves were then compared with room-temperature data from the Bushveld specimen, and the lattice parameters for each curve were raised or lowered where necessary to obtain agreement without changing the transition temperature. The relatively large adjustments, probably due to the approximate compositional estimates, included decreases of $a$ and $\beta$ for augite, and an increase of $\beta$ for pigeonite. The $c$ value of augite, and $a$ and $c$ of pigeonite were not changed substantially from the interpolated curves. The resulting curves, labelled "Bushveld" in Figures 2 and 3, were then accepted, with some misgiving, as representing the correct relations between unit-cell parameters and temperature for the compositions $Wo_{44}$ and $Wo_2$, respectively, on the model Bushveld join.

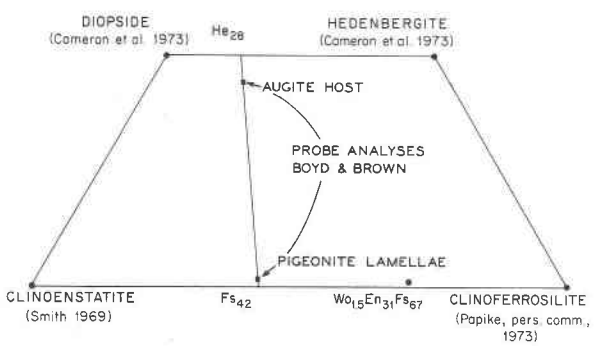


Fig. 7. Pyroxene quadrilateral showing composition of Bushveld augite host and pigeonite I lamellae. Also showing are pyroxene compositions for which high temperature unit-cell parameters have been measured.

Parts A, B, and C of Figure 8 show the relations between $a$, $c$, and $\beta$ respectively as a function of temperature ($T$) and percent Wo along the model Bushveld join. Parameters and temperatures from the "Bushveld" curves in Figures 2 and 3 are plotted along the line $Wo_{44}$ and $Wo_2$ respectively in each part. Adjusted room-temperature parameters are plotted along each base. Contours are drawn based on this information and on a rough estimate of the position of the $P2_1/c \rightarrow C2/c$ transition. Although they are based on very limited data, these diagrams show how further high-temperature and pressure measurements of pyroxene lattices could be put to use, and also demonstrate the need for a quantitative model that will describe accurately the relationships between temperature, pressure, composition, and unit-cell parameters of clinopyroxenes (*e.g.*, Ohashi and Burnham, 1973). The approximate position of the augite–pigeonite strain-free solvus and its metastable extension on the low calcium side was estimated from data of Smith (1972) and Ross *et al.* (1973).

The relationships shown in Figure 8 can be used in several ways. The pure thermal-expansion effects can be evaluated independent of any solvus when one uses the data for $Wo_{44}$ and $Wo_2$ at different temperatures. These values can be compared with results obtained when the solvus shown or any other solvus is used. Comparisons can be made by examining the variations of $\Delta a$, $\Delta c$, and $\Delta\beta$ as temperature changes as in Figure 9, or by examination of the calculated angles of hypothetical phase boundaries as in Figure 10. In both these figures, the effect of the solvus is insignificant below 600°C, modest at intermediate $T$, and large at high $T$ as expected. Figure 9 shows that the "crossing temperature" where $a_{AUG} = a_{PIG}$ (~790°C) is not the same as the "crossing temperature" where $c_{AUG} = c_{PIG}$ (~710°C) and neither coincide with the $P2_1/c \leftrightarrows C2/c$ inversion temperature. Thus, between 790°C and 710°C a region exists where $a_{AUG} > a_{PIG}$ and $c_{AUG} < c_{PIG}$, as surmised by Robinson *et al.* (1971, Fig. 8). Patterns of "001" and "100" exsolution lamellae will be of three different

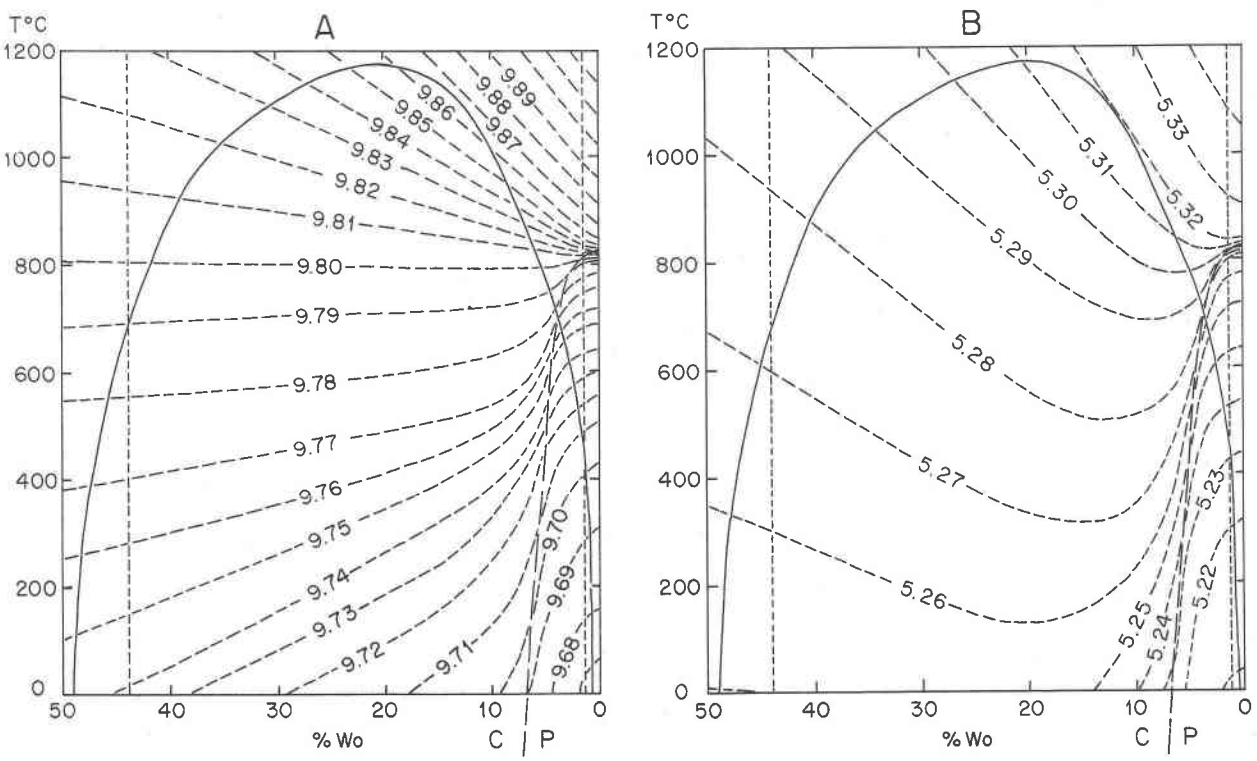


Fig. 8. Model lattice parameters for Bushveld augite and pigeonite lamellae on the join $Di_{72}He_{28}$–$En_{58}Fs_{42}$ as a function of temperature. Boundary of $P2_1/c$ field shown by long-dashed lines. Short-dashed vertical lines indicate Bushveld compositions $Wo_2$ and $Wo_{44}$ used in modeling. (A) Temperature–composition diagram showing contours of $a$. (B) Temperature–composition diagram showing contours of $c$.

types, depending on whether the lamellae form above, within, or below the temperature limits of this region as illustrated in Figure 8D.

When one uses the thermal model presented here, recognizing its likelihood of error and assuming heterogeneous nucleation and growth of pigeonite with compositions lying on a strain-free solvus, the Pig-I (103°) lamellae nucleate at about 1000°C, the Pig "100" (−6°) at about 850°C, Pig-II at 800°C, and Pig-III at 560°C.

Another approach to thermal modeling of the Bushveld specimen is to make direct, high temperature, lattice measurements of host and lamellae, using an automated single-crystal diffractometer. Crystal 1A was examined at 300°, 600°, and 900°C by means of techniques previously described (Smyth, 1974). The results, together with calculated phase boundaries, are given in Table 5. These results agree with the previous model in suggesting that Pig-III lamellae formed at or below 600°C, but disagree with the model at higher temperature in that, at 900°C $a_{AUG} > a_{PIG}$, $c_{AUG} > c_{PIG}$, and the symmetry of pigeonite is still $P2_1/c$. Possibly the thermal model is grossly in error, particularly in estimating the $P2_1/c \leftrightarrows C2/c$ transition temperature. More probably in these short heating experiments the pigeonite lamellae, constrained elastically by the host and now containing abundant faults, are unable to equilibrate chemically, and so do not mimic the lattice parameters they had at the time of nucleation. From the nature of optimal or exact phase boundaries, the orientation of which depends on parameters at nucleation, clearly the most successful temperature predictions will be based on future measurements at temperature and pressure on unconstrained, homogeneous, single crystals close in composition to the natural material under study.

### Lattice orientation and the behavior of high temperature lamellae after exsolution

An important aspect of the formation of exact phase boundaries is the "phase-boundary lattice rotation" discussed above. For model "001" boundaries in pyroxenes on the model Bushveld join, this rotation, in terms of $a_{PIG}$ $\Lambda a_{AUG}$, ranges from +0.22° for room-temperature data to −0.09° for 1150°C data.

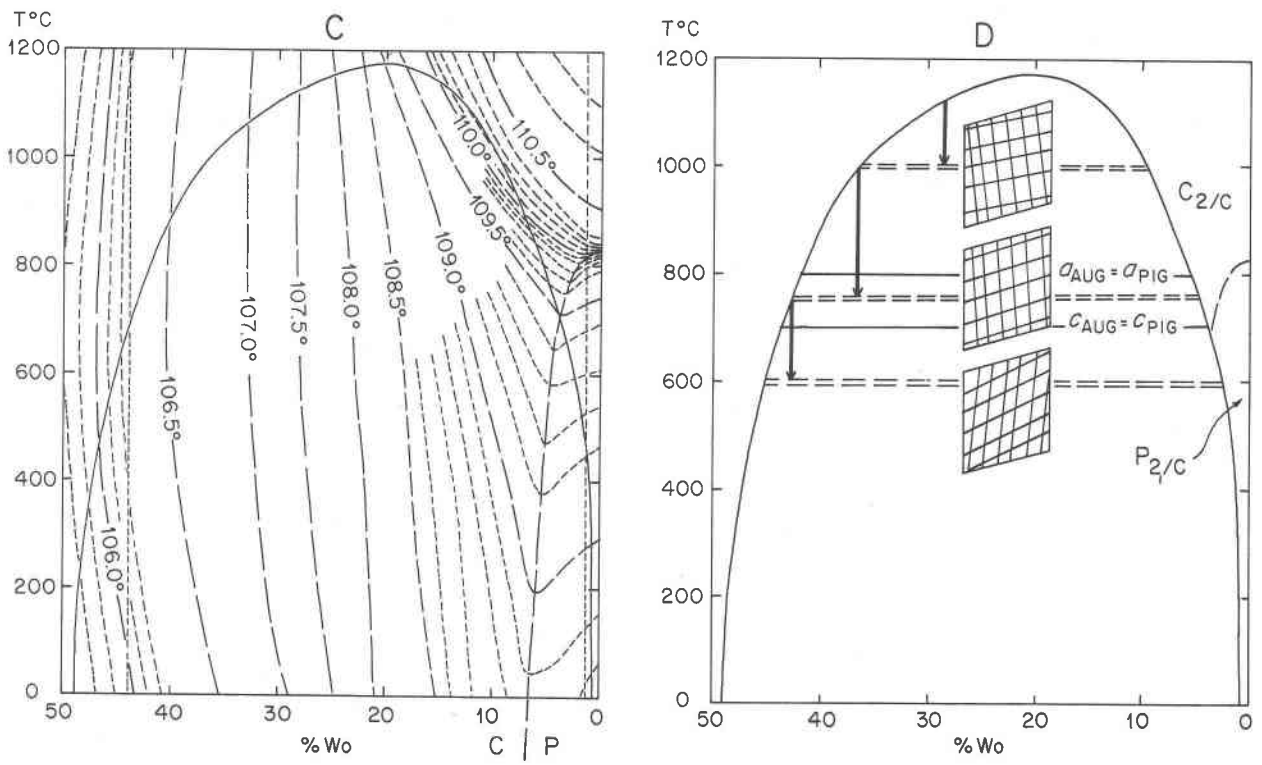


Fig. 8. Continued. (C) Temperature–composition diagram showing contours of $\beta$. (D) Temperature–composition diagram showing temperatures where $a_{AUG} = a_{PIG}$ and $c_{AUG} = c_{PIG}$ and patterns of "001" and "100" lamellae expected to form above, between, and below these temperatures.

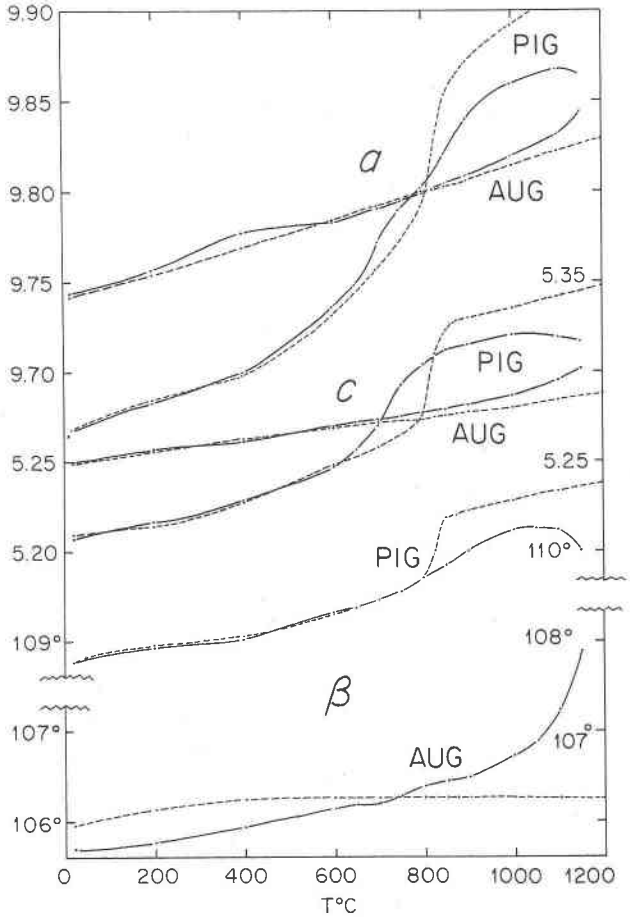


Fig. 9. Comparison of $a$, $c$, and $\beta$ of model augite and pigeonite on the Bushveld join including (long dash dot) and excluding (short dash dot) the effect of the binodal solvus.

On the other hand, the single crystal photographs give angles of $a_{PIG}\Lambda a_{AUG}$ of $-1.03°$ ($-0.80$ to $-1.21°$) for Pig-I lamellae and $-0.65°$ for Pig II, much higher than any of the model values (Table 6, Figure 11). The angles are in the correct negative sense for phase boundaries formed at high temperature (as in Fig. 1B), and so helped identify the reflections belonging to Pig-I and Pig-II, but the amount of the rotation is too large to be accounted for solely by phase-boundary lattice rotation using any reasonable set of high temperature lattice parameters. Hence, this abnormal negative rotation, also reported by Morimoto and Tokonami (1969) in Skaergaard pigeonite (0.9°), by Takeda (1972) in Moore County pigeonite ($-1.5°$), and by McCallum (1974) in Stillwater augite ($-1.5°$), was believed to be the product of some sort of deformation effect that took place after phase separation. Numerous attempts to understand this effect ended in failure until detailed electron micrographs were obtained.

Electron micrographs of a 5 $\mu$m Pig-I lamella, a 1 $\mu$m Pig-II lamellae, and a 0.8 $\mu$m Pig-III lamella are shown in Figure 12. The most striking feature within all three kinds of pigeonite lamellae is the abundant thin (100) stacking faults. In this case the faulting of the 9A monoclinic cell produces an 18A wide orthorhombic cell; a strip of orthopyroxene. The sense of shear is the reverse of that for the $Pbca \rightarrow P2_1/c$ transition as discussed by Coe and Kirby (1975). Their experiments indicate the transition is mechanically reversible, *i.e.* $P2_1/c \rightarrow Pbca$, and the faults are most likely induced by differential contraction of the augite host and its pigeonite lamellae. Quite incidentally, the faults on (100) permit accurate location of the $c$-crystallographic axis of the pigeonite within the lamella, and hence permit accurate measurement of the angles of phase boundaries against the augite host with reference to the pigeonite lattice

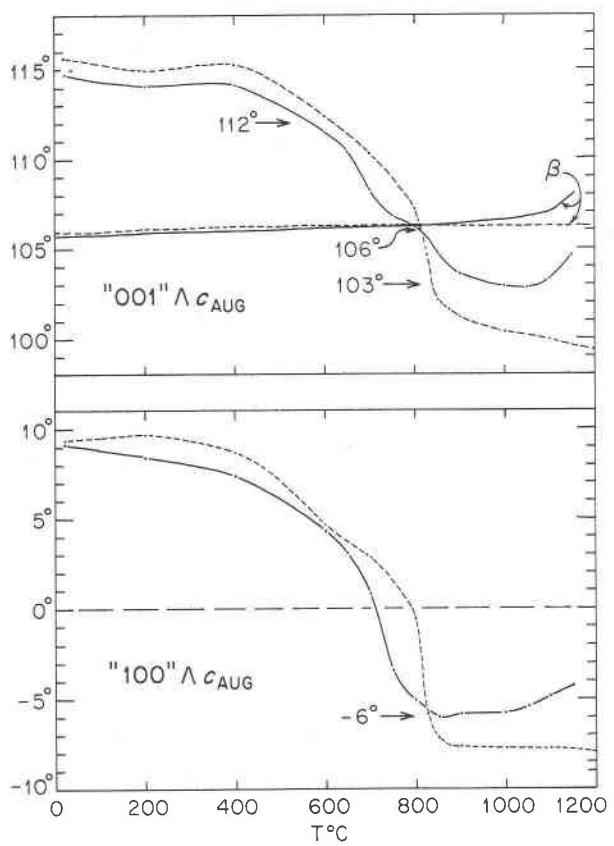


Fig. 10. Model angles of pigeonite exsolution lamellae in augite with respect to temperature ($T$) including (long dash dot) and excluding (short dash dot) the solvus effect. Angles observed in the Bushveld specimen are indicated.

of the lamella. These angles are 107° for Pig-I lamellae, 109° for Pig-II lamellae, and 114° for Pig-III lamellae (Table 4). In terms of model phase boundaries, these angles are exactly compatible with angles of 103°, 106°, and 112° measured with reference to *c* of the augite host.

The abundance of (100) faults appearing within "001" pigeonite lamellae appears to be function of lamella thickness and thus temperature of formation. The faults are most abundant in the thickest pigeonite lamellae. The three electron micrographs gave average numbers of faults per $\mu$m length of 45 for Pig-I, 30 for Pig-II, and 4 for Pig-III. If the density of (100) faults is a function of the amount of lattice deformation a pigeonite lamella has undergone since formation, faults would be expected to be more abundant in early-formed thick lamellae with a long cooling history than in late-formed thin lamellae. An idea of the amount of lattice deformation the pigeonite itself must undergo internally in about 1000°C of cooling is gained by comparing room-temperature lattice parameters of pigeonite with model lattice parameters at high temperature (Table 7). The largest change is the decrease in $\beta$ of pigeonite by about 1.5 degrees, whereas the $\beta$ of the augite host decreases by only about half as much. How can a pigeonite lamella previously locked into an augite host change its angle $\beta$ by 1.5 degrees whereas the host changes its $\beta$ by only half as much?

A key clue to the answer to this question comes from close examination of the boundaries of pigeonite "001" lamellae in the electron micrographs. These show that the boundaries are offset at their intersections with the (100) faults, producing what are, in effect, normal faults. The fault vector has been determined to be 5/6[001], producing a displacement of ~4.5A at the boundary (P.E. Champness, oral communication, 1976). Because it is impossible for the $\beta$ angle of a whole pigeonite lamella to decrease simultaneously, except to the extent that the $\beta$ angle of the augite host also decreases, the lamella apparently breaks up into segments bounded by the (100) faults. Each segment is then relatively free to decrease its $\beta$ by twisting (001) with respect to a fixed (100) and thus to put less strain on the phase boundary. The greater the $\beta$ decrease of pigeonite over that of host

Table 5. Unit-cell parameter measurements of Bushveld augite crystal 1A and included pigeonite lamellae at various temperatures

| 20°C | a | b | c | β | Δa | Δb | Δc | Δβ | (Calculated) "001" Angle | (Calculated) "100" Angle |
|---|---|---|---|---|---|---|---|---|---|---|
| Augite Host | 9.721 | 8.905 | 5.240 | 105.95° | | | | | | |
| Pig I | 9.640 | 8.906 | 5.196 | 108.90° | 0.081 | -0.001 | 0.044 | 2.95° | 116.1° | 10.2° |
| Pig III | 9.633 | 8.906 | 5.194 | 109.00° | 0.088 | -0.001 | 0.046 | 3.05° | 116.6° | 10.4° |
| 300°C | | | | | | | | | | |
| Augite Host | 9.732 | 8.930 | 5.246 | 106.00° | | | | | | |
| Pig I | 9.673 | 8.938 | 5.206 | 109.00° | 0.059 | -0.008 | 0.040 | 3.00° | 113.2° | 8.9° |
| Pig III | 9.676 | 8.937 | 5.204 | 109.08° | 0.056 | -0.007 | 0.042 | 3.08° | 112.6° | 9.1° |
| 600°C | | | | | | | | | | |
| Augite Host | 9.757 | 8.972 | 5.263 | 106.00° | | | | | | |
| Pig I | 9.702 | 8.971 | 5.229 | 109.07° | 0.055 | 0.001 | 0.034 | 3.07° | 112.4° | 7.3° |
| Pig III | 9.705 | 8.978 | 5.228 | 109.00° | 0.052 | -0.006 | 0.035 | 3.00° | 112.2° | 7.7° |
| 900°C | | | | | | | | | | |
| Augite Host | 9.772 | 8.999 | 5.276 | 106.10° | | | | | | |
| Pig I | 9.750 | 8.993 | 5.258 | 109.38° | 0.022 | 0.006 | 0.018 | 3.28° | 108.4° | 3.5° |
| Pig III | 9.749 | 8.978 | 5.259 | 109.45° | 0.023 | 0.007 | 0.017 | 3.35° | 108.5° | 3.2° |

Table 6. Observed and model orientation data of pigeonite lamellae in Bushveld augite host

| Crystal 1A | Observed $a_{PIG}\,\Lambda\,a_{AUG}$ | Model $a_{PIG}\,\Lambda\,a_{AUG}$* | $d\beta_{PIG}-d\beta_{AUG}$** | Observed $c_{PIG}\,\Lambda\,c_{AUG}$ | $\Delta\beta_{Orig.}$# | $\Delta\beta_{Orig.}+d\beta_{PIG}-d\beta_{AUG}$## |
|---|---|---|---|---|---|---|
| Pig I | -1.03° | (1000°C) -0.05° | -0.98° | 3.85° | 3.80° | 2.82° |
| Pig II | -0.65° | (800°C) 0.00° | -0.65° | 3.30° | 3.30° | 2.65° |
| Pig III | +0.08° | (600°C) +0.12° | -0.04° | 2.91° | 3.03° | 2.99° |
| Crystal 3A | | | | | | |
| Pig I | -1.21° | -0.05° | -1.16° | 4.00° | 3.95° | 2.79° |
| Pig III | -0.16° | +0.12° | -0.28° | 3.19° | 3.31° | 3.03° |
| Pig "100" | 3.00° | | | 0.04° | | |
| Crystal 5A | | | | | | |
| Pig I | -0.80° | -0.05° | -0.75° | 3.70° | 3.65° | 2.90° |
| Pig III | +0.10° | +0.12° | -0.02° | 2.88° | 3.00° | 2.98° |
| Pig "100" | 3.09° | | | 0.05° | | |
| Crystal 6A | | | | | | |
| Pig I | -1.05° | -0.05° | -1.00° | 3.75° | 3.70° | 2.70° |
| Pig III | +0.04° | +0.12° | -0.08° | 2.99° | 3.11° | 3.03° |

* "Phase boundary lattice rotation" based on Bushveld model at indicated temperature.

** Amount that β of pigeonite has decreased over the decrease in β of augite host, equivalent to a decrease in Δβ.

# Δβ at original phase separation.

## Original Δβ plus decrease in Δβ (-) is the present Δβ (compare with Table 3).

augite (defined as $d\beta_{PIG}$–$d\beta_{AUG}$), the more numerous are the required faults. This mechanism is illustrated in Figure 13 and evaluated in Table 6. After correction of $a_{PIG}\Lambda a_{AUG}$ for the original phase-boundary lattice rotation (model $a_{PIG}\Lambda a_{AUG}$), the remaining angle, $d\beta_{PIG}$–$d\beta_{AUG}$, is a direct measure of the amount $\beta_{PIG}$ has decreased from $\beta_{AUG}$ since the lamellae formed and could be used as an independent geothermometer, even though the *absolute* amounts of $\beta$-decrease for the two phases are indeterminate. Because the $\beta$-decrease of augite is usually less than 1°, and because the phase boundary is broken into a series of short segments, the original overall trend of the phase boundary itself is preserved during cooling.

Because the relative positions of the *c* axes of pigeonite "001" lamellae and augite host appear not to change after formation, the angle between the *c* axes ($c_{PIG}\Lambda c_{AUG}$, Table 6), after adjustment for phase-boundary lattice rotation (model $a_{PIG}\Lambda a_{AUG}$), should be of the value of $\Delta\beta$ under the conditions of formation ($\Delta\beta_{orig.}$). This value can be applied directly to a figure such as 8C to obtain a determination of temperature. The adjusted value for the original $\Delta\beta$, less the adjusted amount of $\beta$-decrease for pigeonite over that for augite ($\Delta\beta_{orig.} + d\beta_{PIG} - d\beta_{AUG}$), is equal to the present $\Delta\beta$ within close limits (compare Table 6 with Table 3). On the basis of the limited information available, we have not been able to formulate a satisfactory analogous model to explain the lattice orientations of the Pig "100" lamellae also listed in Table 6.

The abundance of (100) stacking faults may also limit the growth of "001" pigeonite lamellae in augite. As lamellar growth in pyroxenes probably proceeds by propagating ledges along the lamellar interface, the presence of partial dislocations at the ends of the faults with Burgers vectors not in that interface, may impede the movement of the ledges. Thus, for example, after Pig-I lamellae develop a high enough density of (100) faults during cooling and growth is reduced, Pig-II lamellae nucleate and grow in the supersaturated regions between the Pig-I la-

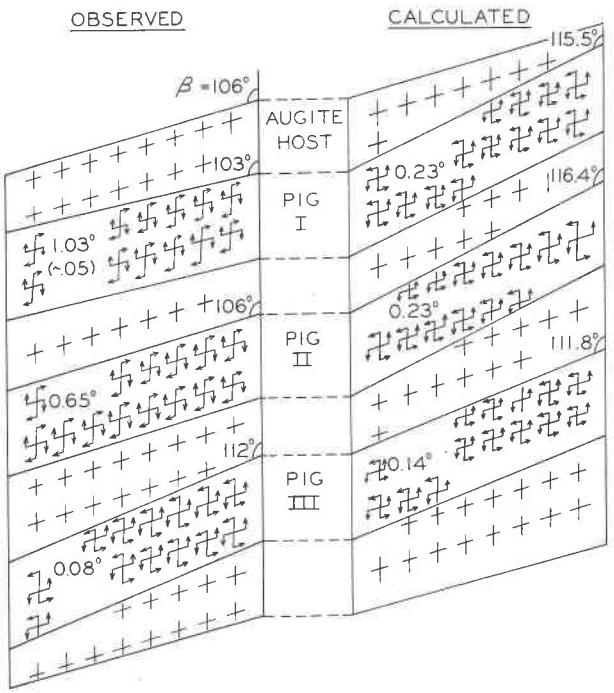


Fig. 11. Observed and calculated phase boundaries and lattice rotations ($a_{PIG} \Lambda a_{AUG}$) for "001" pigeonite lamellae in Bushveld augite crystal 1A. Boundaries calculated from room-temperature parameters for Pig I and II bear little relation to observed angles, showing that the phase boundaries are a fossil of higher-temperature conditions. Similarity of calculated and observed angles for Pig III indicates relatively little change in parameters since Pig III lamellae nucleated.

mellae. A similar sequence occurs for Pig-II and Pig-III lamellae. This corresponds to the observed distribution of the lamellae and points out the possible importance of interface controlled growth in pyroxenes.

The production of stacking faults on (100) to enable a $\beta$ change in pigeonite constrained by an augite host may also be extended to include high temperature host pigeonites and, in some crystals, high-temperature host augites constrained by a host rock, as seen in specimens from Labrador shown to us by Hope M. Davies, University of Massachusetts. Such faults and their partial dislocations may provide the avenues necessary for reconstructive transformation to orthopyroxene, particularly in cases where the product orthopyroxene is not systematically oriented with respect to the original pigeonite.

## Conclusions

A simplified geometric model has been presented for pyroxene exsolution where a monoclinic phase exsolves from a monoclinic host and the *b* dimensions

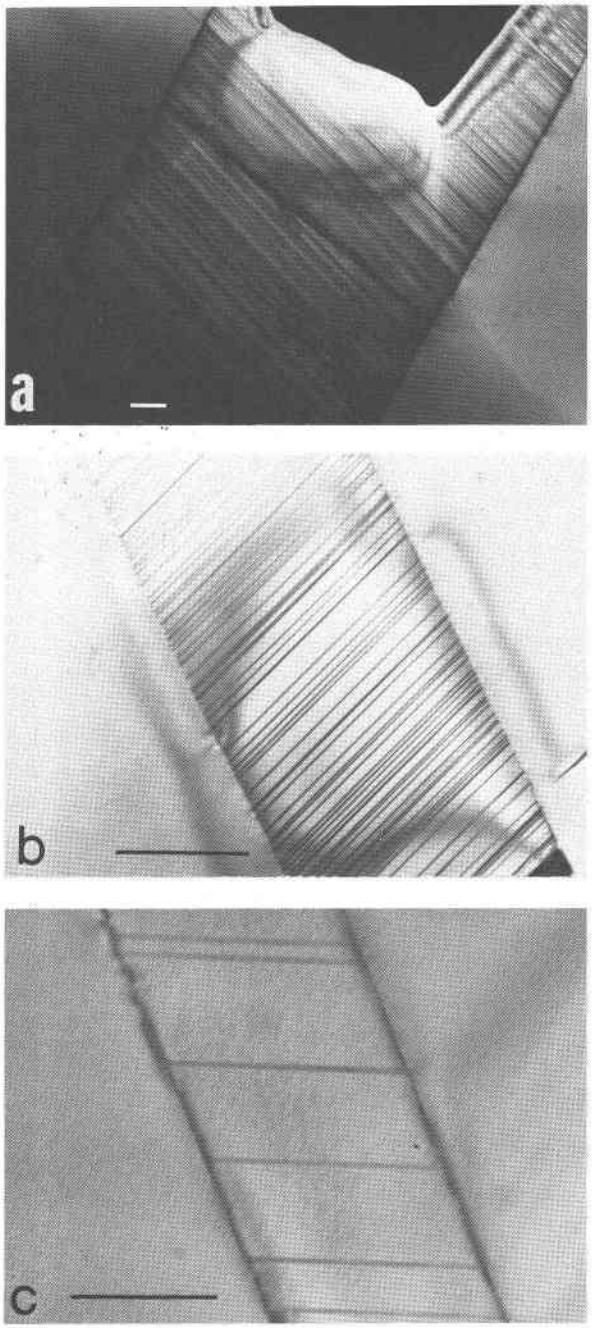


Fig. 12. Transmission electron micrographs of pigeonite lamellae in augite from sample SA-1019. (a) A 5 $\mu$m wide lamella with a high density of (100) stacking faults ["001" interface $\Lambda$ (100) faults = 107°]. Taken in dark field, the black area at top is the edge of the specimen. (b) A 1 $\mu$m wide lamella with (100) faults ["001" interface $\Lambda$ (100) faults = 109°]. (c) A 0.8 $\mu$m wide pigeonite lamella with six (100) stacking faults in the field of view ["001" interface $\Lambda$ (100) faults = 114°]. All of the above were taken at 200 kV with $\vec{g}$ = 201. Scale bar equals 0.5 $\mu$m.

Table 7. Effect of cooling on unit-cell parameters of pigeonite and augite formed at high temperature

| | a | c | β |
|---|---|---|---|
| Bushveld Model Pig, 1000°C | 9.859 | 5.320 | 110.22° |
| Natural Pig~I Lamella, Room Temperature | 9.669 | 5.208 | 108.78° |
| Change during Cooling | -0.190 | -0.112 | -1.44° |
| Bushveld Model Aug 1000° | 9.818 | 5.287 | 106.75° |
| Natural Augite Host, Room Temperature | 9.742 | 5.254 | 105.96° |
| Change during Cooling | -0.076 | 0.033 | -0.79° |

remain identical. This model, when used with high temperature lattice parameters, predicts the "exact phase boundaries" of the lamellar phase at nucleation and thus serves as a geothermometer for natural specimens. The observed "001" boundaries correlate well with those calculated from the model. Because of the $C2/c \rightarrow P2_1/c$ transition the unit cell of pigeonite changes more rapidly during cooling than that of augite, severely straining the lamellae. This strain is relieved by faulting on (100), permitting $\beta$ of pigeonite within each faulted lamella segment to decrease to low temperature values. The amount of $\beta$-decrease of the pigeonite lamellae and the fault density may, therefore, be correlated to the temperature of pigeonite formation providing a second geothermometer. In addition, the faults may inhibit growth of the lamellae. Such a possibility should be considered by those researchers attempting to model lamella growth rates by considering bulk diffusion rates alone.

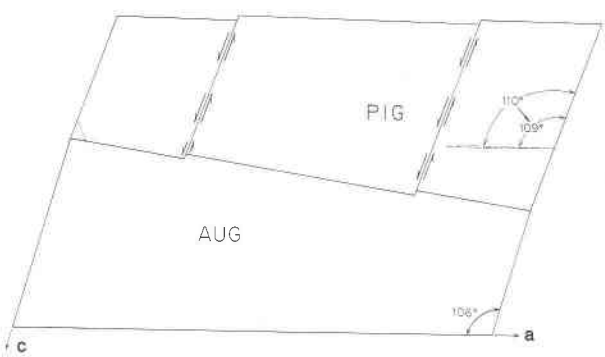


Fig. 13. Diagrammatic view of model "001" interface between high-temperature pigeonite lamella and augite host after cooling. One degree decrease of the pigeonite $\beta$ from 110° and 109° during cooling has been accomodated by development of a series of (100) stacking faults. Although augite and pigeonite lattices are strained where the faults terminate, $\beta$ of pigeonite within the areas bounded by the faults can adjust without straining the entire augite lattice, and the *average* angle of the phase boundary remains essentially unchanged. The greater the amount of $\beta$ decrease in pigeonite, the greater the number of stacking faults needed to accomodate it.

## Acknowledgments

Optical work, computations, and manuscript preparation at the University of Massachusetts were supported by NSF Grant GA-31989 (to Jaffe and Robinson). Robert J. Tracy devised the computer program for calculating phase boundaries from lattice parameters. Part of the drafting was accomplished by Marie Litterer, and manuscript and tables were typed by Maureen Konernak and Virginia van Gessel. Room-temperature X-ray single-crystal studies and electron microscopy were done at the U. S. Geological Survey, Washington, D. C., and Reston, Virginia. High temperature X-ray single-crystal studies were done at the Lunar Science Institute, Houston, Texas. F. R. Boyd, Geophysical Laboratory, Washington, D. C., and G. M. Brown, University of Durham, England, furnished a thin section and rock chip on which most of the work is based. Unpublished data on pyroxenes from Labrador were provided by J. H. Berg, Hope M. Davies, and W. A. Rewinski (University of Massachusetts). Reviews by J. R. Clark and S. Kirby of the U. S. Geological Survey are greatly appreciated. To each of these institutions and persons, we express our grateful acknowledgment.

## Appendix: orientation of the *exact phase boundary*

Consider two monoclinic phases, for example augite (AUG) and pigeonite (PIG), which have identical $b$-dimensions, similar crystal structures, and are intergrown so that their (010) planes are parallel. An *exact phase boundary* between the two intergrown phases is a plane oriented parallel to the common $b$-direction and which contains a special vector $\mathbf{Y}$ directed parallel to the common (010) plane. The magnitude of the unit-repeat of vector $\mathbf{Y}$ in terms of the augite and pigeonite unit-cell parameters is given by

$$(1)\quad |\mathbf{Y}|_{AUG} = (a^2_{AUG}x^2_{AUG} + c^2_{AUG}z^2_{AUG} + 2a_{AUG}c_{AUG}\cos\beta_{AUG}x_{AUG}z_{AUG})^{1/2}$$

and

$$(2)\quad |\mathbf{Y}|_{PIG} = (a^2_{PIG}x^2_{PIG} + c^2_{PIG}z^2_{PIG} + 2a_{PIG}c_{PIG}\cos\beta_{PIG}x_{PIG}z_{PIG})^{1/2}$$

where $x$ and $z$ are coordinates of the vector $\mathbf{Y}$ in the $a$ and $c$ directions, respectively, and $a$, $c$, and $\beta$ are the unit-cell parameters at the temperature of initial phase separation. To provide an "exact lattice match" (coherence) at the phase boundary, the coincident vectors $\mathbf{Y}_{AUG}$ AND $\mathbf{Y}_{PIG}$ must be equal in magnitude; thus

$$(3)\quad |\mathbf{Y}|_{AUG} = |\mathbf{Y}|_{PIG}$$

In addition, there must be structural continuity across the phase boundary, which implies that there be an optimal match of the two crystal structures in the boundary region. This "best structural match," which gives a minimum energy of atomic misfit at the boundary, is obtained when the $x$ and $z$ coordinates of the vectors $\mathbf{Y}_{AUG}$ and $\mathbf{Y}_{PIG}$ are equal; thus

$$(4)\quad x_{AUG} = x_{PIG} \text{ and } z_{AUG} = z_{PIG}$$

Equating (1) and (2) and setting $z = 1$

$$(5)\quad (a^2_{AUG} - a^2_{PIG})x^2 + (2a_{AUG}c_{AUG}\cos\beta_{AUG} - 2a_{PIG}c_{PIG}\cos\beta_{PIG})x + (c^2_{AUG} - c^2_{PIG}) = 0$$

which is of the form

$$Ax^2 + Bx + C = 0 \tag{6}$$

Solving for the two real values of $x$ gives the two possible orientations ("001" and "100") of the exact phase boundary

$$x = [-B \pm (B^2 - 4AC)^{1/2}]/2A \tag{7}$$

The intercepts of the two possible boundary planes with the *a*, *b*, and *c* axes are thus $x_1, y = \infty, z = 1$ and $x_2, y = \infty, z = 1$.[4] If $x < -1$ or $x > 1$, the phase boundary is defined as having an "001" orientation. If $-1 < x < 1$ the phase boundary is defined as having a "100" orientation.

The orientation of the phase boundary, as defined by the acute angle formed between the vector **Y** and the *a* or *c* axis of a particular phase, is given by

$$a_i\Lambda\mathbf{Y} = \pm\sin^{-1}\left(\frac{c_i \sin\beta_i}{|\mathbf{Y}|}\right) \tag{8}$$

and

$$c_i\Lambda\mathbf{Y} = \pm\sin^{-1}\left(\frac{a_i \sin\beta_i\,|x|}{|\mathbf{Y}|}\right) \tag{9}$$

where

$$|\mathbf{Y}| = [(a_i x)^2 + c_i^2 + 2a_i c_i x \cos\beta_i]^{1/2} \tag{10}$$

and $a_i$, $c_i$, and $\beta_i$ refer to the unit-cell parameters of augite or pigeonite.

If $x > 0$, the vector **Y** is directed toward the *obtuse* $\beta$ of augite or pigeonite (between the $+a$ and $+c$ directions, Fig. 1B, 1D) and the angles $a_i\Lambda\mathbf{Y}$ and $c_i\Lambda\mathbf{Y}$ given by (8) and (9) are defined as *negative*. If $x < 0$, the vector **Y** is directed toward the *acute* $\beta$ of augite or pigeonite (between the $-a$ and $+c$ directions, Fig. 1A, 1C) and the angles $a_i\Lambda\mathbf{Y}$ and $c_i\Lambda\mathbf{Y}$ are defined as *positive*.

The angle of relative rotation ($r$) of the lattice of pigeonite with respect to augite for the "100" and "001" type boundaries is defined by

$$r_{100} = c_{\mathrm{AUG}}\Lambda\mathbf{Y} - c_{\mathrm{PIG}}\Lambda\mathbf{Y} \tag{11}$$

and

$$r_{001} = a_{\mathrm{AUG}}\Lambda\mathbf{Y} - a_{\mathrm{PIG}}\Lambda\mathbf{Y}, \tag{12}$$

respectively.

## References


Aaronson, H. I., C. Laird and K. R. Kinsman (1970) Mechanisms of diffusional growth of precipitate crystals. In *Phase Transformations*, p. 313–394. American Society for Metals, Metals Park, Ohio.

Bollmann, W. and H.-U. Nissen (1968) A study of optimal phase boundaries: the case of exsolved alkali feldspars. *Acta Crystallogr., A24,* 546–557.

Boyd, F. R. and G. M. Brown (1969) Electron-probe study of pyroxene exsolution. *Mineral. Soc. Am. Spec. Pap., 2,* 211–216.

Cameron, M., S. Sueno, C. T. Prewitt and J. J. Papike (1973) High temperature crystal chemistry of acmite, diopside, hedenbergite, jadeite, spodumene, and ureyite. *Am. Mineral., 58,* 594–618.

Champness, P. E. and G. W. Lorimer (1973) Precipitation (exsolution) in an orthopyroxene. *J. Materials Sci., 8,* 467–474.

——— and P. A. Copley (1976) The transformation of pigeonite to orthopyroxene. In H.-R. Wenk, Ed., *Electron Microscopy in Mineralogy,* p. 228–233. Springer-Verlag, New York.

Christian, J. W. (1965) *The Theory of Transformations in Metals and Alloys.* Pergamon Press, New York, 973 p.

Coe, R. S. and S. H. Kirby (1975) The orthoenstatite to clinoenstatite transformation by shearing and reversion by annealing: mechanism and potential applications. *Contrib. Mineral. Petrol., 52,* 29–56.

Copley, P. A., P. H. Champness and G. W. Lorimer (1974) Electron petrography of exsolution textures in an iron-rich clinopyroxene. *J. Petrol., 15,* 41–57.

Gittos, M. F., G. W. Lorimer and P. E. Champness (1974) An electron-microscopic study of precipitation (exsolution) in an amphibole (the hornblende–grunerite system). *J. Mater. Sci., 9,* 184–192.

Hess, H. H. (1960) Stillwater igneous complex, Montana. *Geol. Soc. Am. Mem., 80,* 230 p.

Jaffe, H. W., P. Robinson, R. J. Tracy and M. Ross (1975) Orientation of pigeonite lamellae in metamorphic augite: correlation with composition and calculated optimal phase boundaries. *Am. Mineral., 60,* 9–28.

McCallum, I. S. (1974) Exsolution and inversion in Stillwater pyroxenes (abstr.). *Trans. Am. Geophys. Union, 55,* 468.

Morimoto, N. and M. Tokanami (1969) Oriented exsolution of augite in pigeonite. *Am. Mineral., 54,* 1101–1117.

Ohashi, Y. and C. W. Burnham (1973) Clinopyroxene lattice deformations: the roles of chemical substitution and temperature. *Am. Mineral., 58,* 843–849.

Prewitt, C. T., G. E. Brown and J. J. Papike (1971) Apollo 12 clinopyroxenes: High temperature X-ray diffraction studies. *Proc. Second Lunar Science Conf., 1,* 59–68.

Robinson, P., H. W. Jaffe, M. Ross and C. Klein, Jr. (1971) Orientation of exsolution lamellae in clinopyroxenes and clinoamphiboles: consideration of optimal phase boundaries, *Am. Mineral., 56,* 909–939.

Ross, M. and J. S. Huebner (1975) A pyroxene geothermometer based on composition–temperature relationships of naturally occurring orthopyroxene, pigeonite, and augite (abstr.) *Extended Abstracts,* Int. Conf. Geothermometry Geobarometry, Pennsylvania State University.

———, ——— and E. Dowty (1973) Delineation of the one atmosphere augite–pigeonite miscibility gap for pyroxenes from lunar basalt 12021. *Am. Mineral., 58,* 619–635.

———, P. Robinson and H. W. Jaffe (1972) Pigeonite lamellae in Bushveld augite sequentially exsolved on phase boundaries at angles controlled by differential contraction (abstr.). *Geol. Soc. Am. Abstr. with Programs, 4,* 644–645.

Smith, D. (1972) Stability of iron-rich pyroxene in the system $CaSiO_3$–$FeSiO_3$–$MgSiO_3$. *Am. Mineral., 57,* 1413–1428.

Smith, J. V. (1969) Crystal structure and stability of the $MgSiO_3$ polymorphs; physical properties and phase relations of Mg, Fe pyroxenes. *Mineral. Soc. Am. Spec. Pap., 2,* 3–29.

Smyth, J. R. (1974) The high temperature crystal chemistry of clinohypersthene. *Am. Mineral., 59,* 1069–1082.

Takeda, H. (1972) Exsolution and stacking disorder in some meteoritic and lunar pyroxenes (abstr.). *Geol. Soc. Am. Abstr. with Programs, 4,* no. 7, 684.

Turnock, A. C., D. H. Lindsley and J. E. Grover (1973) Synthesis and unit-cell parameters of Ca–Mg–Fe pyroxenes. *Am. Mineral., 58,* 50–59.

Willaime, C. and W. L. Brown (1974) A coherent elastic model for the determination of the orientation of exsolution boundaries: application of feldspars. *Acta Crystallogr., A30,* 316–331.


*Manuscript received, October 28, 1976; accepted for publication, May 18, 1977.*

[4] If $a_{\mathrm{AUG}} = a_{\mathrm{PIG}}$, $x_1 = -\infty$, $x_2 = -C/B$